Characteristic low-field magnetic response of granular superconductors

T. Di Matteo [a,*], A. Tuohimaa [a], J. Paasi [a], R. de Luca [b]

[a] *Laboratory of Electricity and Magnetism, Tampere University of Technology, P.O. Box 692, FIN-33101 Tampere, Finland*
[b] *INFM-Dipartimento di Fisica, Universita' degli Studi di Salerno, I-84081 Baronissi Salerno, Italy*

Abstract

The low-field magnetic response of a physical system consisting of eight superconducting spherical grains in a cubic arrangement is studied by means of a three-dimensional Josephson junction network. The lower threshold field for this system is numerically studied as a function of the inclination of the externally applied magnetic field $\vec{H}$ with respect to the z-axis. © 1998 Published by Elsevier Science B.V. All rights reserved.

1. Introduction

Granularity in high-T_c superconductors has led to novel types of physical phenomena [1–3], some of which have not found a complete explanation yet. Indeed, the interplay between intergranular and intragranular properties of these systems makes it difficult to interpret their low-field magnetic response [4].

As far as the intergranular properties of granular superconductors are concerned, weak coupling between superconducting grains gives rise to the so called 'intergranular critical state' [5–8]. In order to fully understand the flux penetration mechanisms underlying this type of response, we begin by considering a very simple system consisting of eight superconducting spherical grains in a cubic arrangement. We carry out our investigation in the low-field and low-temperature limit in such a way that intragranular flux penetration can be neglected. By showing that this system can be studied by means of a Josephson junction network consisting of twelve junctions located at the sides of a cube, we give a one to one correspondence between observed physical quantities and calculated ones by introducing an effective inductance matrix which takes into account the magnetic energy of the circulating currents. Basic magnetic response of the cubic junction network has been treated elsewhere [9]. In the present paper we numerically evaluate the lower threshold field intensity for flux

---

* Corresponding author. Fax: +358-3365-2160; E-mail: tiziana@vaxsa.csied.unisa.it

penetration in a homogeneous cubic network for arbitrary field orientations and for different values of the coupling parameter $\tilde{\beta} = L_{eff} I_J / \Phi_0$, where L_{eff} is the effective inductance parameter, Φ_0 is the elementary flux quantum and I_J is the maximum Josephson current of the junctions. It is found that, as in the case of one junction in a single superconducting ring, there exists a critical value $\tilde{\beta}_c$ of the coupling parameter $\tilde{\beta}$, below which flux penetration is reversible. Moreover, for a fixed $\tilde{\beta}$ value, the first threshold field intensity is seen to decrease for increasing values of the inclination of the field direction with respect to the z-axis in the interval $[0, \pi/4]$.

2. Current and flux distributions

In the present section we shall give a schematic representation of current and flux distributions in the physical system of Fig. 1a in the case the superconducting grains are taken to be perfectly diamagnetic and identical. In the simpler case when the external field is applied along a symmetry axis of the cubic structures, the z-axis for example, we might picture the current distribution as in Fig. 1b. In this case, indeed, only azimuthal currents flow in the model system, and we might distinguish them as external and internal shielding currents, which we shall denote as I and i, respectively. The internal shielding currents circulating in the lower and upper part of the system will be denoted as i_{low} and i_{up}. Similarly, the external shielding currents will be denoted as I_{low} and I_{up}, if they circulate in the lower or upper part of the system. In the same way, we can define the fluxes linked to the upper inner and outer loops as Φ_{up} and Θ_{up} and the corresponding fluxes linked to the lower inner and outer loops as Φ_{low} and Θ_{low}. By taking into account both self-inductance and mutual inductance effects, we can write the following:

$$\begin{aligned}
\Phi_{up} &= l i_{up} + m^* I_{up} + m i_{low} + m' I_{low} + \mu_0 H S_{in}, \\
\Theta_{up} &= m^* i_{up} + L I_{up} + m' i_{low} + M I_{low} + \mu_0 H S_{out}, \\
\Phi_{low} &= m i_{up} + m' I_{up} + l i_{low} + m^* I_{low} + \mu_0 H S_{in}, \\
\Theta_{low} &= m' i_{up} + M I_{up} + m^* i_{low} + L I_{low} + \mu_0 H S_{out}.
\end{aligned} \tag{1}$$

In Eq. (1) the inductance coefficient matrix is taken in such a way that the self-inductances relative to a single loop are denoted by l for inner loops of area S_{in} and by L for outer loops of area S_{out}; the mutual inductances, instead, are taken to be M for outer–outer and m for inner–inner loop current interaction. The coefficients m^* and m', on the other hand, denote inner–outer (or outer–inner) loop current interactions for loops lying on the same face and for loops lying in different parallel faces, respectively. Since the grains have been assumed to be in the perfect Meissner state, we can set:

$$\begin{aligned}
\Theta_{up} &= \Phi_{up} = \Phi, \\
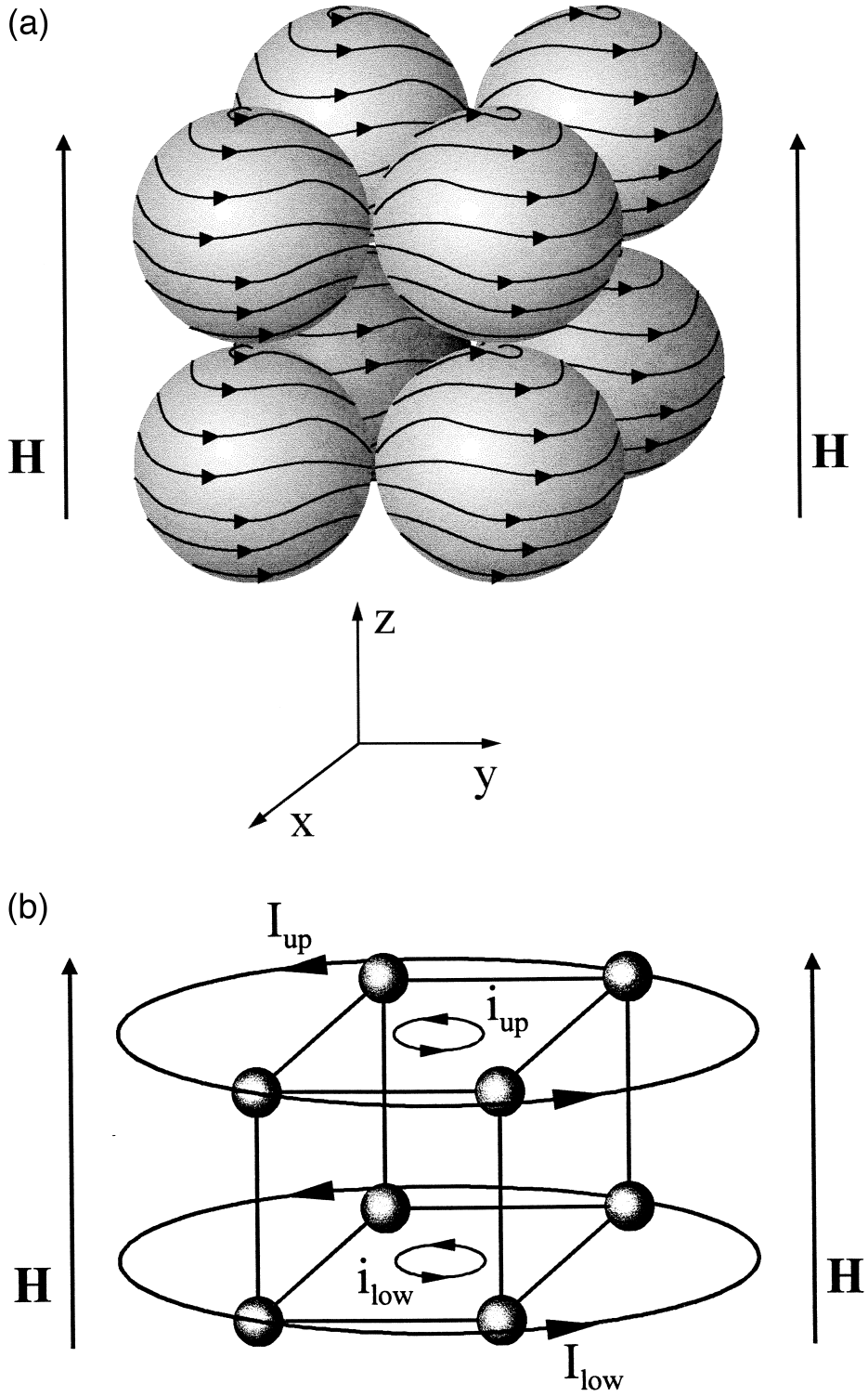\Theta_{low} &= \Phi_{low} = \Phi'.
\end{aligned} \tag{2}$$

Furthermore, by symmetry reasons, we can write:

$$\begin{aligned}
\Phi &= \Phi', \\
I_{up} &= I_{low} = I, \\
i_{up} &= i_{low} = i.
\end{aligned} \tag{3}$$

In this way, Eq. (1) reduce to the following:

$$\begin{aligned}
\Phi &= (m^* + m')i + (L + M)I + \mu_0 H S_{out}, \\
\Phi &= (l + m)i + (m^* + m')I + \mu_0 H S_{in}.
\end{aligned} \tag{4}$$

We can now solve Eq. (4) in terms of the currents i and I and define the current circulating in the upper and

lower junctions as $I^{(B)} = i + I$. We shall see in what follows that this current is just the effective current flowing in the Josephson junctions (JJ's) connecting the grains. Therefore, from Eq. (4) we can write the following:

$$\Phi = L_{eff} I^{(B)} + \mu_0 H S_{eff}, \tag{5}$$

where

$$L_{eff} = \frac{(L+M)(l+m) - (m^* + m')^2}{(L+M) + (l+m) - 2(m^* + m')} \tag{6}$$

and

$$S_{eff} = \frac{[(L+M) - (m^* + m')]S_{in} + [(l+m) - (m^* + m')]S_{out}}{(L+M) + (l+m) - 2(m^* + m')} \tag{7}$$

are the effective self-inductance and mutual inductance coefficients of a single representative loop of the schematic current distributions in Fig. 1b. In this way, the 3D physical system has been reduced to a model system consisting of a single superconducting loop interrupted by four JJ's.

In the case the external field is along an arbitrary direction in space, we could express the fluxes in terms of the circulating current by introducing additional elements to the inductance matrix, whose complete structure could be summarized as follows:

$$P_{(\eta\xi)}^{(\mu\nu)}(\vec{r},\vec{r}') = \left[\delta_{\vec{r},\vec{r}'} L + (1 - \delta_{\vec{r},\vec{r}'})M\right]\delta_{(\mu\nu),(\eta\xi)} + [-1]^{(\delta_{\vec{r},\vec{r}'})}M_0\left[1 - \delta_{(\mu\nu),(\eta\xi)}\right], \tag{8}$$

$$T_{(\eta\xi)}^{(\mu\nu)}(\vec{r},\vec{r}') = \left[\delta_{\vec{r},\vec{r}'} l + (1 - \delta_{\vec{r},\vec{r}'})m\right]\delta_{(\mu\nu),(\eta\xi)} + [-1]^{(\delta_{\vec{r},\vec{r}'})}m_0\left[1 - \delta_{(\mu\nu),(\eta\xi)}\right], \tag{9}$$

$$R_{(\eta\xi)}^{(\mu\nu)}(\vec{r},\vec{r}') = \left[\delta_{\vec{r},\vec{r}'} m^* + (1 - \delta_{\vec{r},\vec{r}'})m'\right]\delta_{(\mu\nu),(\eta\xi)} + [-1]^{(\delta_{\vec{r},\vec{r}'})}m'_0\left[1 - \delta_{(\mu\nu),(\eta\xi)}\right], \tag{10}$$

where the elements of the matrix P are relative to outer-outer loop current interactions, those of the matrix T pertain to inner-inner loop current interactions, and those of the matrix R pertain to inner-outer loop current interactions. In addition, the $\vec{r}$ and $\vec{r}'$ have been introduced to give account of the position of the unit cell for the system, consisting of three faces in the three planar orientations in space, namely, (yz), (xz), and (xy). In the case of a single cube the only possible positions of the unit cell are at the origin ($\vec{r} = 0$) and at a $\hat{\xi}$, $\hat{\xi}$ being the unit vector in the direction of the ξ-axis ($\xi = (x,y,z)$) and a being the length of the cube side. In Eqs. (8)–(10), the double greek indices are taken to represent the three planar orientations in space. We have tried to keep the notation similar to that used above with the coefficients M_o, m_o, and m'_o being the mutual inductances between orthogonal faces for outer–outer, inner–inner and inner–outer (or outer–inner) loop current interactions, respectively. We can define the inner and outer loop currents flowing in the ($\eta\xi$) plane as $i_{(\eta\xi)}(\vec{r})$ and $I_{(\eta\xi)}(\vec{r})$, so that the corresponding fluxes $\Phi_{(\eta\xi)}(\vec{r})$ and $\Phi_{(\eta\xi)}(\vec{r})$ could be written in the following compact form:

$$\Phi_{\eta\xi}(\vec{r}) = \sum_{\vec{r}'}\sum_{\mu\nu} R_{(\eta\xi)}^{(\mu\nu)}(\vec{r},\vec{r}') I_{(\mu\nu)}(\vec{r}') + \sum_{\vec{r}'}\sum_{\mu\nu} T_{(\eta\xi)}^{(\mu\nu)}(\vec{r},\vec{r}') i_{(\mu\nu)}(\vec{r}') + \mu_0 \vec{H} \cdot \vec{s}_{(\eta\xi)}(\vec{r}), \tag{11}$$

$$\Theta_{\eta\xi}(\vec{r}) = \sum_{\vec{r}'}\sum_{\mu\nu} P_{(\eta\xi)}^{(\mu\nu)}(\vec{r},\vec{r}') I_{(\mu\nu)}(\vec{r}') + \sum_{\vec{r}'}\sum_{\mu\nu} R_{(\eta\xi)}^{(\mu\nu)}(\vec{r},\vec{r}') i_{(\mu\nu)}(\vec{r}') + \mu_0 \vec{H} \cdot \vec{S}_{(\eta\xi)}(\vec{r}), \tag{12}$$

where $\vec{S}_{(\eta\xi)}$ and $\vec{s}_{(\eta\xi)}$ are the area vectors associated to the outer and inner loops, and orthogonal to the $\eta-\xi$ plane, respectively. Again, by having assumed the grains to be in the perfect Meissner state, we can set:

$$\Phi_{(\eta\xi)}(\vec{r}) = \Theta_{(\eta\xi)}(\vec{r}) \tag{13}$$

as it was done in the simpler case treated before. We have thus obtained a linear system of equations, which

Fig. 1. (a) Current distribution in an eight-grains system in a cubic arrangement. The applied field is orthogonal to the base face of the cubic structure; (b) Schematic representation of the current distribution shown in (a).

could be solved for the currents in such a way that an effective current $I_{(\mu\nu)}^{(B)}(\vec{r}) = I_{(\mu\nu)}(\vec{r}) + i_{(\mu\nu)}(\vec{r})$ could still be defined. In this way, a one to one correspondence between the effective currents $I_{(\mu\nu)}^{(B)}$ and the fluxes has been obtained through the inductance matrices. If the magnetic response of a real physical system is to be described, one first needs to solve Eqs. (11,12) for the $I_{(\mu\nu)}$'s and the $i_{(\mu\nu)}$'s in terms of the applied fluxes $\mu_0 \vec{H} \cdot \vec{S}_{(\mu\nu)}$ and $\mu_0 \vec{H} \cdot \vec{s}_{(\mu\nu)}$ and of the $\Phi_{(\mu\nu)}$'s. Secondly, one defines $I_{(\mu\nu)}^{(B)}(\vec{r}) = I_{(\mu\nu)}(\vec{r}) + i_{(\mu\nu)}(\vec{r})$ so that the effective currents are expressed in terms of the fluxes by means of an effective mutual inductance matrix, which we shall call $A_{(\eta\xi)}^{(\mu\nu)}(\vec{r},\vec{r}')$, and by an effective area vector $\vec{S}_{(\eta\xi)}^{eff}(\vec{r})$, as it was done in the case of an axial externally applied field. In this way, one may finally write:

$$\Phi_{(\eta\xi)}(\vec{r}) - \mu_0 \vec{H} \cdot \vec{S}_{(\eta\xi)}^{eff}(\vec{r}) = \sum_{\vec{r}'} \sum_{\mu\nu} A_{(\eta\xi)}^{(\mu\nu)}(\vec{r},\vec{r}') I_{(\mu\nu)}^{(B)}(\vec{r}'). \tag{14}$$

However, because of the complexity of the space distribution of currents in the real system of Fig. 1a, we shall here only consider one characteristic low-field response, whose qualitative behavior does not depend on the particular choice of the inductance matrices; namely, the lower threshold field. Let us then consider the case in which the inductance matrices are taken to be equal:

$$P_{(\eta\xi)}^{(\mu\nu)}(\vec{r},\vec{r}') = T_{(\eta\xi)}^{(\mu\nu)}(\vec{r},\vec{r}') = R_{(\eta\xi)}^{(\mu\nu)}(\vec{r},\vec{r}') \tag{15}$$

and for $\vec{S}_{(\eta\xi)}(\vec{r}) = \vec{s}_{(\eta\xi)}(\vec{r})$. Eqs. (11) and (12) will therefore reduce to the following:

$$\Phi_{(\eta\xi)}(\vec{r}) - \mu_0 \vec{H} \cdot \vec{S}_{(\eta\xi)}(\vec{r}) = \sum_{\vec{r}'} \sum_{\mu\nu} P_{(\eta\xi)}^{(\mu\nu)}(\vec{r},\vec{r}') I_{(\mu\nu)}^{(B)}(\vec{r}'). \tag{16}$$

In this case, obviously, the grains reduce to points, while the effective areas are taken to be finite, so that the link to the real system, whose electrodynamic equations are given by Eqs. (11) and (12), is lost. However, Eq. (16) more easily describes the connection between the effective current flowing into the junctions and the flux linked to the superconducting loops in the system.

3. The Josephson junction network

In Section 2 we have written down the equations describing the classical electrodynamic response of the system in Fig. 1a without any mention of its superconducting quantum behavior. However, we have derived an expression for the fluxes $\Phi_{(\mu\nu)}$ in terms of the currents $I_{(\mu\nu)}^{(B)}$, which we defined to be the effective currents flowing in the junctions and which can be readily used when the Josephson equations are invoked. Indeed, by associating a Josephson junction to each contact point between grains, one obtains a cubic network consisting of twelve Josephson junctions, one at each side of the cube. With the aid of the RSJ model [10], now, by introducing the non-linear Josephson operator defined as:

$$O_J(\cdot) = \frac{\Phi_0}{2\pi R} \frac{\mathrm{d}}{\mathrm{d}t}(\cdot) + I_J \sin(\cdot), \tag{17}$$

where R is the junction's resistive parameter, for each junction in the network we can write [9]:

$$O_J\left[\varphi_\xi(\vec{r})\right] = \sum_{\mu,\nu} \epsilon_{\xi\mu\nu}\left(I_{(\xi\nu)}^{(B)}(\vec{r}) - I_{(\xi\nu)}^{(B)}(\vec{r} - a'\hat{\nu})\right), \tag{18}$$

where $\varphi_\xi(\vec{r})$ is the gauge-invariant superconducting phase difference pertaining to a junction lying in the ξ-direction and located in a unit cell at point $\vec{r}$. In Eq. (18) $\epsilon_{\eta\mu\nu}$ is the Levi Civita's symbol and a' is the effective length of the cube side. Notice also that the summation is carried out over all possible $(\mu\nu)$'s, but that only (yz), (xz) and (xy) terms contribute to it.

In addition to the Josephson equations describing phase dynamics, we may invoke the Bohm–Aharonov relation, which, when written for a closed superconducting path containing Josephson junctions, relates the phase differences of the junctions in the closed path and the flux linked to it, so that [9]:

$$2\pi\Phi_{(\eta\xi)}(\vec{r})/\Phi_0 = 2\pi n_{(\eta\xi)}(\vec{r}) + \varphi_\xi(\vec{r} + a\hat{\eta}) - \varphi_\xi(\vec{r}) - \varphi_\eta(\vec{r} + a\hat{\xi}) + \varphi_\eta(\vec{r}), \tag{19}$$

where $n_{(\eta\xi)}(\vec{r})$ are integers and, again, $(\eta\xi)$ takes on the following form: (yz), (xz), (xy). Eqs. (16)–(19) completely define the magnetic response of the system. In this way we may start analyzing one of the most peculiar characteristics of granular superconductors; namely, the lower threshold field. Indeed, when a granular superconductor and, in particular, the cubic system under study is cooled below the critical temperature of the grains in the absence of externally applied fields (ZFC), no flux is present in the superconducting system itself. In this way, given the absence of currents, we may set all the superconducting phase differences to zero, so that all the integer values $n_{(\eta\xi)}(\vec{r})$ may be taken to be exactly null in Eq. (19). When a magnetic field is subsequently applied, external shielding currents will tend to exclude flux lines from the inner part of the sample. However, Josephson junctions located in the external shielding current path may suffer a 2π phase slip if the current value exceeds I_J. For each 2π phase slip in one junction, Eq. (19) predicts the penetration of one flux quantum into the inner intergranular region of the system, i.e., the normal region enclosed in the superconducting granular system. This penetration mechanism may be either reversible or irreversible, depending on the values of the characteristic parameter $\tilde{\beta} = L_{eff} I_J / \Phi_0$, L_{eff} being the effective inductance of the loop the flux links to. Indeed, as in the more usual d.c. SQUID case, if $\tilde{\beta} < \tilde{\beta}_c$, flux penetration is reversible, whereas, if $\tilde{\beta} \geq \tilde{\beta}_c$, the system irreversibly traps flux lines in its intergranular region.

In the case the external field is applied in the direction of the symmetry axis of the cubic system, it can be shown [9] that $\tilde{\beta}_c = 2/\pi$. The irreversible magnetic behavior for $\tilde{\beta} \geq \tilde{\beta}_c$ may be detected, for example, in the $\Phi_{(xy)}$ vs. $\Phi_{ex} = \mu_0 H S_0^{eff}$ curves, S_0^{eff} being the effective area of one cube face. Indeed, in Fig. 2 we show the normalized flux $\Psi_{(xy)} = \Phi_{(xy)}/\Phi_0$ as a function of the normalized applied flux $\Psi_{ex} = \Phi_{ex}/\Phi_0$ for a system in which the mutual inductance matrices have been taken to satisfy Eq. (15). In this case $L_{eff} = l + m$, and we took $\beta = l I_J / \Phi_0 = 1$ and $m/l = 0.03$, as calculated elsewhere [9]. Moreover, I_J has been taken not to depend on the externally applied field. Since $\tilde{\beta} = 1.03\beta > \tilde{\beta}_c$, the system shows an irreversible flux transition at $\Psi_{ex} = \Psi_{ex}^{(1)}$, recognizable by a first discontinuity in the $\Psi_{(xy)}$ vs. Ψ_{ex} curve by following this curve from $\Psi_{ex} = 0$ and for increasing values of the externally applied flux. The lower threshold flux $\Psi_{ex}^{(1)}$ can be obtained analytically in this case [9], so that:

$$\Psi_{ex}^{(1)} = \tilde{\beta}\sqrt{1 - \left(\frac{2}{\pi\tilde{\beta}}\right)^2} + \frac{2}{\pi}\left(\pi - \sin^{-1}\sqrt{1 - \left(\frac{2}{\pi\tilde{\beta}}\right)^2}\right). \tag{20}$$

A hysteretic behavior is also detectable in Fig. 2. In Fig. 3, we finally show the current $i_{(xy)}^{(B)} = I_{(xy)}^{(B)}/I_J$ as a
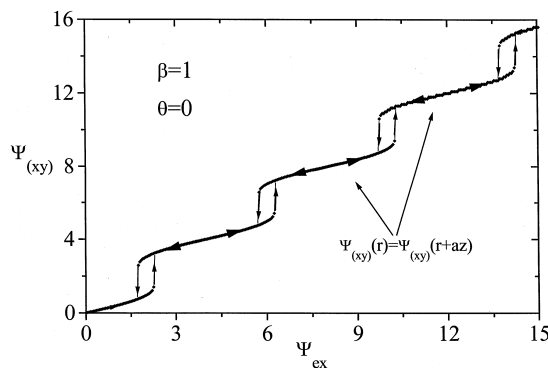

Fig. 2. Flux linked to the (xy) faces as a function of the normalized applied flux Ψ_{ex} for $\beta = 1.0$ and for $\theta = 0$. For a quick conversion to non-normalized quantities, by taking $S_0^{eff} \simeq 100$ μm^2, we have $\mu_0 H \simeq 0.02$ Ψ_{ex} [mT].
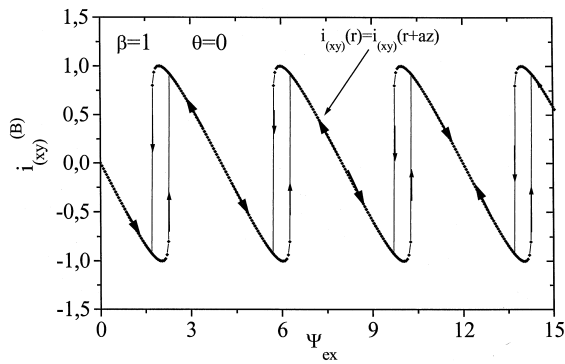
Fig. 3. Mesh current circulating in the (xy) faces as a function of the normalized applied flux Ψ_{ex} for $\beta = 1.0$ and $\theta = 0$.

function of Ψ_{ex} for $\beta = 1$. The 2π phase slip of the junctions lying in the faces orthogonal to the field direction generates here a current inversion from negative to positive values at $\Psi_{ex} = \Psi_{ex}^{(1)}$.

4. Lower threshold field

When the external field is applied along an arbitrary direction in space, shielding currents circulate in all cubic faces, so that an exact analytic solution for the lower threshold field $\Psi_{ex}^{(1)}$ is not feasible anymore. In this general case one needs to numerically integrate the dynamical equations for the cubic system, starting from ZFC conditions and letting the externally applied flux to increase a small enough variation $\Delta\Psi_{ex}$. In this way one records the lower threshold field value by detecting the first discontinuity of amplitude greater than one flux quantum in the $\Psi_{(\mu\nu)}$ vs. Ψ_{ex} curves, or, equivalently, the first current discontinuity in the $i_{(\mu\nu)}^{(B)}$ vs. Ψ_{ex} graphs. In what follows we shall take an applied magnetic field $\vec{H}$ lying in the y–z plane and making an angle θ with the z-axis. A resulting $\Psi_{ex}^{(1)}$ vs. θ graph is shown in Fig. 4 for various values of the parameter β. In this curves $m/l = 0.03$ and $m_0/l = -0.24$. Let us take the maximum Josephson current of the junctions not to depend on the externally applied flux. Therefore, we can consider the $\Psi_{ex}^{(1)}$ vs. θ curves for a fixed β value as representing the θ-dependence of the lower threshold field at constant temperature. The lowering of these curves for decreasing β values may thus be interpreted as an effect of the decrease of the superconducting coupling energy due to increasing temperatures. The decrease of $\Psi_{ex}^{(1)}$ with increasing θ-values in the interval $[0, \pi/4]$
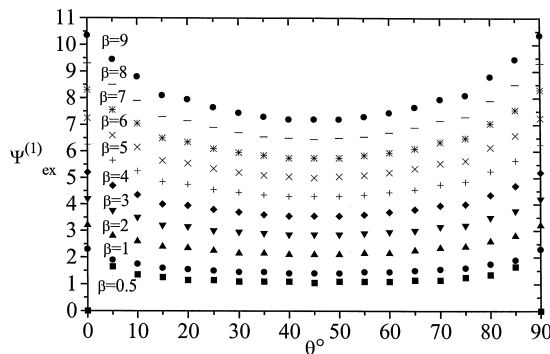

Fig. 4. Angular dependence of the lower threshold field $\Psi_{ex}^{(1)}$ for various values of the parameter β and for $m/l = 0.03$ and $m_0/l = -0.24$.
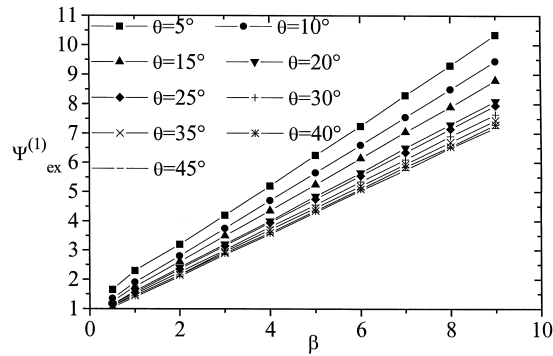
Fig. 5. Lower threshold field $\Psi_{ex}^{(1)}$ as a function of the parameter β for various values of the angle θ and for $m/l = 0.03$ and $m_0/l = -0.24$.

may be explained by noticing that additional currents circulate in the cube faces, so that their combined action tend to add in some junctions and to subtract in other junctions. Of course, phase slips always take place in those junctions where the currents circulating in adjacent loops flow in the same direction. One may also notice that, for $\beta = 0.5$, the lower threshold field does not exist for $\theta = 0$, while it still exists for $\theta \neq 0$. This fact is indicative of an increase of the effective coupling parameter $\tilde{\beta}$ for $\theta \neq 0$, when compared to the case of $\theta = 0$.

In Fig. 5 we report the β-dependence of the lower threshold field for different values of the angle θ. In this figure we may notice a quasi-linear asymptotic dependence of $\Psi_{ex}^{(1)}$ from β, similar to that obtained from the analytic expression for $\theta = 0$ (Eq. (20)) shown elsewhere [9]. For increasing θ-values in the interval $[0, \pi/4]$, we notice a shift of the curves toward lower values of $\Psi_{ex}^{(1)}$ and a corresponding decrease of the slope of the interpolating straight line. We remind that β is a coupling parameter whose temperature dependence is linked to that of I_J through the constant factor L_{eff}/Φ_0. Therefore, being $I_J(T)$ a monotonically decreasing function of T [11,12], we may extract an additional qualitative type of information on these curves; namely, that the lower threshold field $\Psi_{ex}^{(1)}$ is a monotonically decreasing function of T. The behaviour is in a qualitative agreement with experiments done in $YBa_2Cu_3O_x$ [13] and $(Bi,Pb)_2Sr_2Ca_2Cu_3O_y$ [14] granular superconductors.

Quantitative comparison of the calculations with experiments is difficult, mainly for two reasons. A real sample consists of thousands of grains with more or less different grain and intergrain properties. Thus the situation does not correspond well with the model specimen with a few grains of homogeneous properties. Secondly, in the model we suppose that the magnetic flux has not penetrated into the superconducting grains, i.e. the grains are in the Meissner state. This allows us to model pure intergranular properties of the granular material. In many granular superconductors the condition is justified at low magnetic fields and low enough temperatures. However, in high quality material with well oriented grains and strong intergranular links, such as in high-T_c tape superconductors, this may not always be valid and, therefore, experiments done with high quality material may not present solely intergranular properties but an admixture of intergranular and intragranular properties of the material.

5. Conclusion

By examining a homogeneous granular system consisting of eight grains in a cubic arrangement, we have investigated the link existing between this class of superconductors and the Josephson junction network models adopted in the description of the magnetic behavior of granular superconductors. A one to one correspondence between the observed physical quantities in the eight grain system and the corresponding quantities calculated

by means of a cubic Josephson junction network was found to be given by the mutual inductance matrices introduced in defining the classical electrodynamic response of the system.

Furthermore, by considering the simple case in which the obtained inductance matrices are all equal, we have shown the resulting flux and current distribution as a function of the externally applied flux. A lower threshold field for the system has been defined as the external magnetic field value at which the first irreversible flux penetration takes place after ZFC. The lower threshold field behavior has been finally analyzed as a function of the inclination of the applied magnetic field, taken to lie on the y–z symmetry plane, with respect to the z-axis.

Acknowledgements

References

[1] J.G. Bednorz, K.A. Muller, Z. Phys. B 64 (1986) 189.
[2] J.R. Clem, Physica C 153–155 (1988) 50.
[3] M. Tinkham, C.J. Lobb, Solid State Phys. 42 (1989) 91.
[4] J. Paasi, M. Lahtinen, V. Plechácek, Physica C 242 (1995) 267.
[5] D.X. Chen, A. Sanchez, A. Hernando, Phys. Rev. B 50 (1994) 13735.
[6] T. Wolf, A. Majhofer, Phys. Rev. B 47 (1993) 5383.
[7] R. De Luca, S. Pace, G. Raiconi, Phys. Lett. A 172 (1993) 391.
[8] J. Paasi, A. Tuohimaa, J.-T. Eriksson, Physica C 259 (1996) 10.
[9] R. De Luca, T. Di Matteo, A. Tuohimaa, J. Paasi, Phys. Rev. B 57 (1998) 1173.
[10] A. Barone, G. Paternó, Physics and Applications of the Josephson Effect, Wiley, New York, 1982.
[11] V. Ambegaokar, A. Baratoff, Phys. Rev. Lett. 10 (1963) 489.
[12] V. Ambegaokar, A. Baratoff, Errata, Phys. Rev. Lett. 11 (1963) 104.
[13] R.B. Goldfarb, A.F. Clark, A.I. Braginski, A.J. Panson, Cryogenics 27 (1987) 475.
[14] R. Job, M. Rosenberg, Physica C 172 (1991) 391.